PAPER

Density-controlled electrochemical synthesis of ZnO nanowire arrays using nanotextured cathode

IOP Publishing Nanotechnology
Nanotechnology 35 (2024) 185301 (10pp) https://doi.org/10.1088/1361-6528/ad2018

Density-controlled electrochemical synthesis of ZnO nanowire arrays using nanotextured cathode

Hyeonjin Eom[1], Junyoung Hur[2], Sang-Keun Sung[3], Jun-Ho Jeong[4,*] and Inkyu Park[5,*]

[1] Carbon Neutral Technology R&D Department, Korea Institute of Industrial Technology (KITECH), Cheonan-si 31056, Republic of Korea
[2] Department of System Engineering, ITER Korea, Korea Institute of Fusion Energy (KFE), Daejeon 34133, Republic of Korea
[3] Digital Health Care Research Center, Gumi Electronics and Information Technology Research Institute (GERI), Gumi-si 39253, Republic of Korea
[4] Department of Nano Manufacturing Technology, Korea Institute of Machinery & Materials (KIMM), Daejeon 34103, Republic of Korea
[5] Department of Mechanical Engineering and KI for the NanoCentury (KINC), Korea Advanced Institute of Science and Technology (KAIST), Daejeon 34141, Republic of Korea

E-mail: jhjeong@kimm.re.kr and inkyu@kaist.ac.kr

Received 26 October 2023, revised 15 December 2023
Accepted for publication 18 January 2024
Published 15 February 2024

Abstract

Zinc oxide (ZnO) nanowires fabricated via wet chemical synthesis on flexible polymer substrates are inherently unstable against mechanical bending stress because of their high density and weak adhesion to the substrate. We introduce a novel method for controlling the density of such ZnO nanowire arrays using a three-dimensional corrugated metal substrate. These metal substrates, featuring extruded and recessed patterns fabricated via nanoimprint lithography, were employed as cathodes during the electrochemical deposition of ZnO nanowire arrays. The ZnO nanowire arrays synthesized on the patterned metal thin film exhibited smaller diameters and lower densities compared to those on non-patterned metal films. This reduction in density can be attributed to aligned nucleation and limited growth on the patterned metal surface. Crucially, ZnO nanowires synthesized on patterned metal substrates displayed remarkable mechanical robustness against external forces, a direct consequence of their reduced density. In contrast, nanowires synthesized on non-patterned metal substrates were broken under mechanical bending. Detailed morphological analyses performed after mechanical bending tests confirm that ZnO nanowires synthesized on nanoimprinted metal electrodes exhibited enhanced mechanical characteristics compared to those on non-patterned metal electrodes. These findings clearly demonstrate the promise of utilizing density-controlled ZnO nanowires in piezoelectric devices.

Supplementary material for this article is available online

Keywords: zinc oxide nanowire, nucleation, selective electrodeposition, nanoimprinted pattern, piezoelectricity

1. Introduction

Various synthesis methods have been developed for ZnO nanowire arrays, each tailored to achieve specific characteristics in the resulting nanowire structures. Dry-based methods, such as chemical vapor deposition [1, 2], physical vapor deposition [3], and thermal evaporation [4] have been used for fabricating highly crystalline ZnO nanowire arrays. ZnO nanowire arrays synthesized using the dry-based method exhibit high sensitivity to chemicals and stable chemical-reactive functions owing to

* Authors to whom any correspondence should be addressed.

the high crystallinity of the nanostructures [3–6]. For example, the highly crystalline ZnO nanowire arrays fabricated by using the dry-based method exhibit favorable piezoelectric properties because of their high aspect ratio and crystallinity [7–9]. However, drawbacks of these dry-based methods include the requirement for a vacuum system and high synthesis temperatures (typically in the range of 900 °C–1050 °C). These conditions are not ideal for fabricating ZnO nanowires on flexible substrates and controlling their densities. Moreover, the morphological control of ZnO nanowires through dry-based methods heavily relies on the properties of the bilayer acting as the seed layer.

The wet-based methods, on the other hand, have gained significant attention due to their lower synthesis temperatures and vacuum-free processes. The morphology control through wet-based methods, such as hydrothermal [10–12], and electrochemical methods [13–15], has been investigated by adjusting the concentration and temperature of the ZnO precursor because these deposition conditions affect the number of nucleation sites and the preferred growth orientation of the ZnO nanowires. Importantly, the temperatures required for wet-based synthesis (typically in the range of 70 °C–95 °C) are suitable for flexible polymer substrates.

Nonetheless, existing density-controlled synthesis methods for ZnO nanowires based on wet chemical synthesis are limited because densely packed ZnO nanowires are produced owing to their continuous nucleation growth on the surface of two-dimensional substrates and consecutive growth at the nucleation sites. A dense ZnO nanowire array structure is difficult to use in mechanical-electrical transducers because high-density nanowires can be destroyed by external load. To prevent mechanical failure of ZnO nanowires, density-controlled wet-based synthesis of ZnO nanowire arrays on flexible polymer substrates has been explored by patterning the seed layer or marking layer using a photolithography method [16–18].

In addition to these challenges, embedding ZnO nanowires within a polymer matrix, such as polydimethylsiloxane (PDMS), polyvinylidene fluoride (PVDF), and SU-8 epoxy-based photoresist, has been employed to prevent mechanical failure of ZnO nanowire devices [17, 19–21]. In the case of using a polymer matrix for embedding ZnO nanowires, the physical attachment characteristics at the polymer matrix-the ZnO nanowire interface should be considered as well as the physical attachment characteristics at the polymer matrix-electrode interface.

Since the synthesis of the crystalline ZnO nanowire on the electrode of the flexible device without mechanical failures is limited, the transfer method of ZnO nanowires by using carrier substrate has been used for placing the ZnO nanowire on the electrode of the flexible device [22–24].

In a previous study, a metal-nanoimprinted poly(methyl methacrylate) (PMMA) substrate was investigated to enhance the interfacial adhesion between the metal thin film and polymer substrate [25]. Herein, we propose a density-controlled ZnO nanowire electrochemical synthesis method that uses the aforementioned metal-nanoimprinted PMMA substrate [25], to prevent mechanical failure of dense ZnO nanowires, particularly in mechanical transducers. The density and geometrics of ZnO nanowires fabricated on metal-nanoimprinted PMMA substrate were investigated and compared to ZnO nanowires fabricated on metal-plane PMMA substrate. A flexible device containing ZnO nanowires array was fabricated by our proposed density-controlled ZnO nanowire synthesis method and its mechanical and piezoelectric properties were evaluated.

2. Experimental

2.1. Fabrication of metal thin films on nanoimprinted polymer substrates

A commercial PMMA film (SKYSUN Corp. Republic of Korea) was thermally imprinted with a nanoimprinting mold featuring various periodic line array patterns (e.g. 200 nm line width and 400 nm pitch or 100 nm line width and 200 nm pitch) under a pressure of 30 bar at 150 °C for 5 min. To observe the vertical scanning electron microscope (SEM) image of the final structure, a nanoimprint structure was fabricated on the silicon (Si) wafer surface. To evaluate the surface of the final structure, and investigate its flexible mechanical properties and piezoelectric characteristics, the nanoimprinted structure was directly fabricated on the surface of the nanoimprinted PMMA substrate. Subsequently, a gold (Au)/titanium (Ti) dual-layer thin film (with either 100 nm/10 nm or 50 nm/5 nm thickness for the Au/Ti layers) was deposited on the nanoimprinted PMMA substrate via thermal evaporation. Different evaporation angles ($\theta = 0°$ and 60°) were used for the fabrication of two kinds of geometrical metal patterns [26], Au0electrode and Au60electrode, respectively (More details in supplementary information). All metal patterns were created by non-oblique angle deposition ($\theta = 0°$) unless otherwise noted.

2.2. Synthesis of vertical ZnO nanowires on metal deposited nanoimprinted polymer substrates

ZnO nanowires were electrodeposited on the surface of the Au/Ti film, acting as the working electrode in the electrodeposition system. The electrolyte consisted of 1 M sodium nitrate ($NaNO_3$) and 1 mM zinc nitrate ($Zn(NO_3)_2$) in ultrapure water. A three-electrode cell configuration was employed, with a nanoimprinted metal film as the working electrode, a platinum (Pt)-coated Ti plate as the counter electrode, and a silver/silver chloride saturated with potassium chloride (Ag/AgCl (saturated KCl)) electrode as the reference electrode. The electrodeposition was conducted at 80 °C under a stirring rate of 400 rpm, applying a constant potential of −1.0 V for 2 h using a potentiostat/galvanostat (601D, CH Instruments, Inc., USA). After electrodeposition, the sample was rinsed with ultrapure water and dried at 80 °C for 1 h to remove the organic residues.

2.3. Characterization of morphologies and compositions of ZnO nanowires

Surface morphologies were analyzed using a SEM (XL30SFEG, Philips Corporation, Netherlands) and a transmission electron

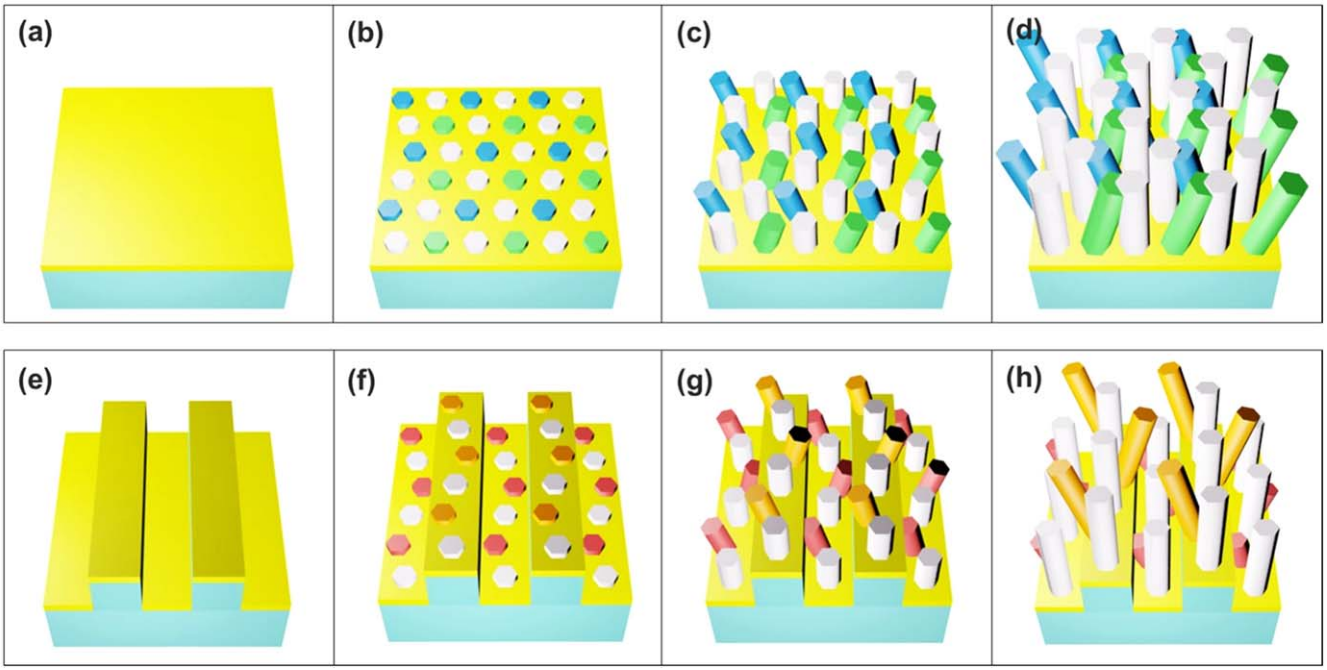

Figure 1. Schematic representation of the ZnO nanowire growth processes on different substrates: (a) deposition of a metal film on a planar polymer substrate, (b) formation of ZnO nuclei, (c) growth of ZnO nanorods, and (d) formation of ZnO nanowire arrays on the planar metal-polymer substrate. (e) Deposition of a metal film on a nanoimprinted polymer substrate, (f) formation of ZnO nuclei, (g) growth of ZnO nanorods, and (h) formation of ZnO nanowire arrays on the nanoimprinted metal-polymer substrate.

microscope (TEM, JEM-ARM200F, JEOL) equipped with a focused ion beam system (FIB, Helios NanoLab, FEI, USA). Composition mapping was conducted using energy dispersive x-ray spectroscopy (EDS). Crystallographic structures were determined by x-ray diffraction (XRD, Rigaku D/max-2500, Japan) with Cu Kα radiation (λ = 1.5405 Å) at 40 kV and 300 mA.

2.4. Fabrication and electrical characterization of piezoelectric nanogenerator

For the top electrode, Ti (20 nm thickness) and Au (200 nm thickness) dual-layer thin films were deposited on top of the ZnO nanowires coated Au/Ti-nanoimprinted PMMA substrate using thermal evaporation. Silver epoxy was used to establish the electrical connection between the electrode and the electrical wire. The piezoelectricity was measured using an electrical measuring instrument (601D, CH Instruments, Inc., USA) within a Faraday cage.

3. Results and discussion

3.1. Mechanism of ZnO nanowire growth on the line-patterned metal film

We describe two conceptual growth processes of ZnO nanowire array structures, each corresponding to a ZnO nanowire array deposition mechanism on the plane metal film and periodic metal film, respectively (see figure 1 for visual representation). At the outset of electrodeposition, nuclei of ZnO nanostructures formed on the metal film's surface due to the selective growth of ZnO nanostructures on the conductive electrode, which acted as the cathode during electrodeposition [27]. On the plane metal film, nuclei of ZnO nanostructures appeared randomly, while on the line-patterned metal film, nuclei exhibited an aligned pattern (see figures 1(b) and (f).

Subsequently, the majority of ZnO nanorods grew vertically, at an angle of 90° with respect to the electrode, while some nanorods exhibited oblique growth patterns, deviating from the 90° orientation because of their preferred crystalline orientation (see figures 1(c) and (g)) [28].

The diameter, shape, and density of the synthesized ZnO nanowires varied depending on the geometry of the cathode as ZnO nanorods grew into ZnO nanowires. On the plane metal film, ZnO nanorods grew predominantly vertically (depicted in white) while some exhibited non-vertical growth directions (depicted in sky blue and green) (see figure 1(c)) Almost all ZnO nanorods synthesized on the plane metal film grew into nanowires with attached ends because of their differing growth directions (see figure 1(d)).

In contrast, aligned ZnO nanorods generated on the line-patterned metal film primarily grew into vertical nanowires with loosely attached ends (see figures 1(g) and (h). On the line-patterned metal film, ZnO nanorods grew vertically (depicted in white), while some deviated from the vertical orientation on the extruded and recessed metal lines (depicted in orange and red, respectively) (see figure 1(g)). Notably, ZnO nanowires grown on the extruded line-patterned metal film exhibited vertical growth without attached ends. The growth of ZnO nanowires in a non-vertical direction of the recessed line-patterned metal film was impeded by the walls of the extruded polymer pattern. This differential growth of

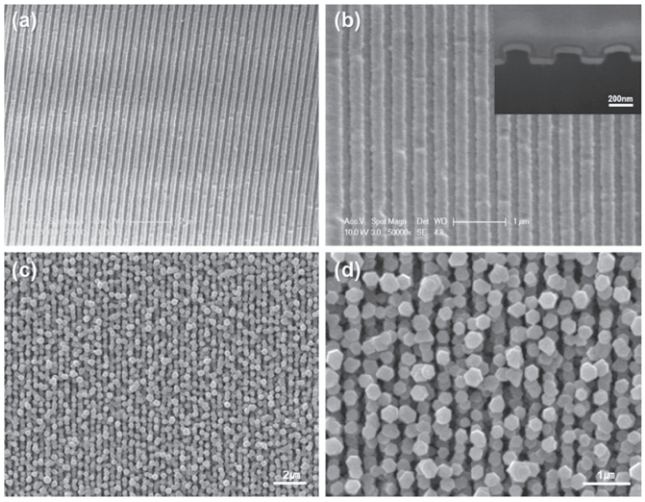

Figure 2. Surface SEM images of (a) and (b) Au(200 nm)/Ti(20 nm) dual-layer film deposited on the nanoimprinted PMMA substrate, with an inset showing a cross-sectional view in (b). (c) And (d) surface SEM images of ZnO nanowires electrodeposited for 30 min on the Au/Ti dual-layer film deposited on the nanoimprinted PMMA substrate.

ZnO nanowires on the line-patterned metal film prevented attachment and, consequently, limited the increase in diameter and density of the ZnO nanowire array structures (see figures 1(g) and (h)).

3.2. Morphologies and compositions

Figures 2(a) and (b) show the surface morphologies of the Au (50 nm)/Ti (5 nm) dual-layer thin film deposited on the nanoimprinted PMMA substrate. The nanoimprinted PMMA substrate exhibits periodic line arrays of rectangular wave patterns with a width of 194 nm, pitch of 408 nm, and height of 113 nm (inset of figure 2(b)). After depositing the Au/Ti dual-layer thin film on a nanoimprinted PMMA substrate via thermal evaporation, the Au/Ti thin films covered the extruded and recessed surfaces of the nanoimprinted PMMA substrate, while leaving the side walls bare because of the directionality of the thermal evaporation process [29]. Figures 2(c) and (d) show the results of the intermediate stage of the ZnO nanowire electrodeposition process on the metal-nanoimprinted polymer substrate. The aligned ZnO nanowire array structure was electrochemically deposited in a relatively short time, approximately 30 min, confirming the selective nucleation and growth of ZnO nanowires on the Au/Ti films deposited on the nanoimprinted PMMA substrate. This selective electrochemical deposition of aligned ZnO nanowires with preferred orientations [28] induces the growth of longer ZnO nanowires with preferred orientations.

High-resolution (HR) cross-sectional TEM images were taken of samples with an identical electrodeposition time (∼30 min) to characterize the distinctive growth process of the ZnO nanowires on the nanoimprinted-structured cathode. ZnO nanowires were prepared on the metal patterns/nanoimprinted polymer/Si substrate to facilitate subsequent analysis and filled with a commercial black-colored permanent marker (Namepen, Monami Co., Republic of Korea) to prevent mechanical failure of the ZnO nanowires during the FIB milling process for sample preparation [30]. Because the ZnO nanowires synthesized on the metal-nanoimprinted PMMA substrate with a width of 200 nm of line pattern experienced horizontal collapse during the FIB milling process, the nanoimprinted polymer-coated Si substrate fabricated by nanoimprint stamp with a width of 100 nm, pitch of 200 nm, and height of 100 nm was utilized for synthesizing and observing the of nanowires in these confined spaces. Clear TEM images of the differential growth of ZnO nanowires synthesized on the patterned substrate with a 100 nm line width are presented in figures 3(a)–(c). As shown in the cross-sectional images, ZnO nanowires are vertically and obliquely grown on the extruded metal patterns, while vertical ZnO nanowires and ZnO nanodot-shaped nanostructures are synthesized on the recessed metal patterns. The infrequent formation of ZnO nanodot-shaped nanostructures on the recessed metal patterns results from the presence of surrounding extruded polymer patterns. The oblique growth characteristics with a preferred orientation of electrochemically synthesized ZnO nanostructures [13, 14, 28], hindered the growth of nanowires in these confined spaces. Conversely, ZnO nuclei synthesized on the extruded metal patterns grew into nanorods/nanowires because of the relatively wider spacing compared to the recessed metal patterns. Figure S3 compares the morphologies of the ZnO nanowires electrodeposited for 2 h at the boundary between the plane metal film and metal patterns. ZnO nanowires deposited on metal patterns exhibit smaller diameters and densities than planar ones because of restricted growth on the recessed pattern, while those deposited on plane metal electrodes show attached ends and higher density. Therefore, the density of ZnO nanowires electrochemically synthesized on metal-nanoimprinted polymer substrates can be controllable because of selective nucleation and the differential growth on the extruded and recessed metal patterns on nanoimprinted polymer substrates.

Figure 4(a) represents a high-angle annular dark field image of electrodeposited ZnO nanowires on the metal-nanoimprinted polymer-coated Si substrate and shows nanowires and nanodots on the extruded and recessed patterns, respectively. EDS maps of the same sample are shown in figures 4(b)–(e). The combination of zinc (Zn), gold (Au), and oxygen (O) exhibits vertical ZnO nanowires and ZnO nanodots on the extruded and recessed Au films, respectively (figure 4(b)). Each Au film fabricated on the extruded and recessed polymer patterns was separated (figure 4(d)). Zn was detected on the surface of the Au metal electrode (figure 4(c)). Clear ZnO crystals on the Au electrodes were observed on the same sample via XRD peak analysis. Crystalline ZnO nanowires were selectively synthesized on metal patterns through electrodeposition (figure S4(b)). Because HR TEM measurement on the surface of the ZnO nanowire was limited by carbon contamination from the polymer substrate (compare figures S5(a)–(c) and (d)–(e)), XRD analysis was conducted to confirm the growth direction of ZnO nanowires deposited on the plane metal film and metal-nanoimprinted polymer.

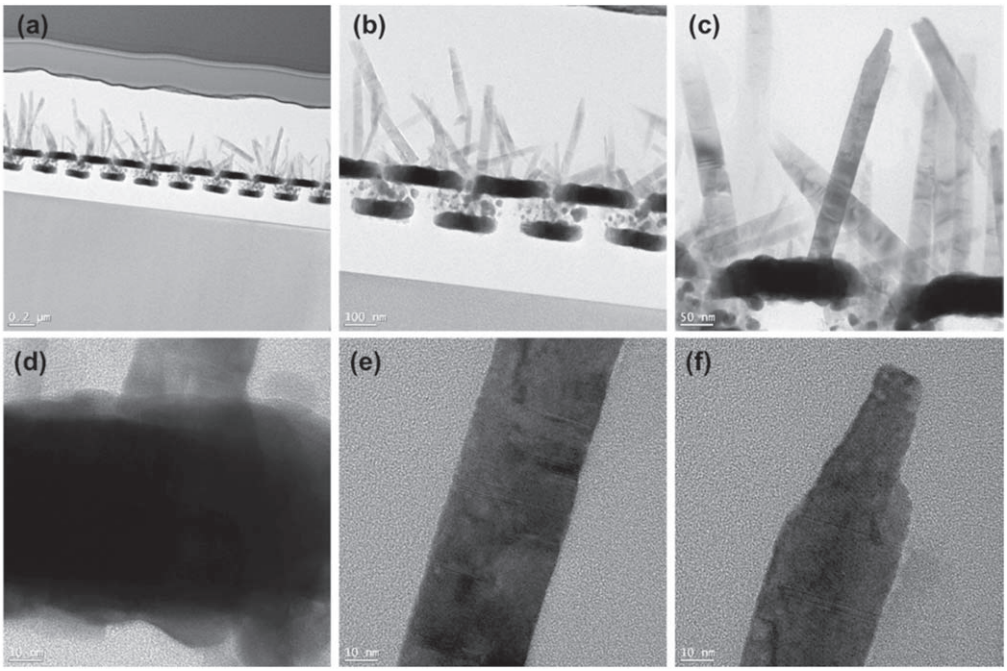

Figure 3. (a)–(c) Cross-sectional TEM images, and (d) high-resolution TEM image at the bottom, (e) middle, and (f) top of ZnO nanowire deposited on the Au/Ti dual-layer thin film/nanoimprinted polymer/Si substrate.

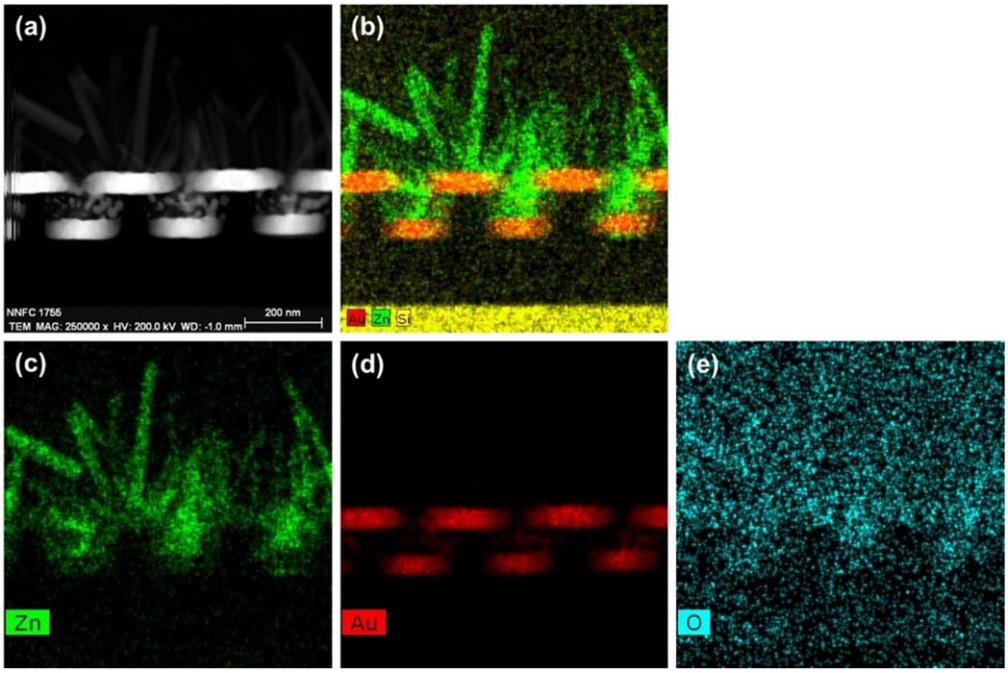

Figure 4. Cross-sectional analysis of the ZnO nanowire on the Au/Ti dual-layer thin film/nanoimprinted polymer/Si substrate using HAADF mode and EDS mapping: (a) HAADF mode image and elemental mapping results for (b) the combined elements, (c) Zn, (d) Au, and (e) O.

The ZnO nanowire grown on the Au/Ti/nanoimprinted PMMA substrate shows a high intensity of (002) peak. This (002) peak matches the wutzite ZnO structure [31]. The growth direction of a ZnO nanowire is [0001], which is the *c*-axis of the wurtzite ZnO crystal. Moreover, the ZnO nanowires with a major peak (002) which is related to the orientation of the ZnO nanowires along this *c*-axis are arranged perpendicular to the substrate [32].

In contrast, the ZnO nanowires grown on a plane metal substrate show a lower (002) peak while representing the highest (103) peak. ZnO nanowires with a major peak (103) are oriented obliquely rather than perpendicular to the substrate [32]. As a result, ZnO nanowires grown on an Au/Ti/nanoimprinted PMMA substrate are almost oriented perpendicular to the substrate, while ZnO nanowires grown on a plane metal substrate are oriented obliquely to the substrate.

Xu *et al* investigated the growth of aligned ZnO nanowire arrays by using an open circle patterned (∼ 100 nm) substrate[16]. In their study, ZnO nanowires were grown on circular patterns during hydrothermal processes, and vertically aligned ZnO nanowires were synthesized because of faster growth in the vertical direction than in the lateral direction. The relatively strong XRD peak of ZnO (002) of their study indicates an almost perfect vertical alignment of the ZnO nanowires. As shown in the SEM and TEM results of our study, the ZnO nanowire arrays were more predominantly electrodeposited on the extruded metal patterns than on the recessed metal pattern. Because the width of the extruded metal pattern is 100 or 200 nm, the nuclei of ZnO nanostructures on the surface of the extruded metal patterns were formed as a seed layer with limited space at the initial electrodeposition step. Single or several ZnO nanowires were grown from the ZnO seed layer which was deposited within a given width of the metal pattern. The nuclei of the ZnO nanowires on the surface of the recessed metal patterns were formed as a seed layer with limited space at the initial electrodeposition step because the width of the recessed metal pattern was also 100 or 200 nm. The ZnO nuclei on the surface of the recessed metal patterns grew shorter nanowires than the ZnO nucleus on the surface of the extruded metal patterns because of the prevention of growth by the side of the walls. This predominantly ZnO nanowire growth on the extruded metal patterns rather than on the recessed metal pattern results in vertical alignment of the ZnO nanowires. The strongest ZnO (002) peak on this sample also indicates the vertical alignment of the ZnO nanowires [16]. Therefore, differences in the nucleus spaces of ZnO nanowires at the initial stage of electrochemical synthesis resulted from the predominant growth on extruded metal patterns than on recessed metal patterns, and faster growth in the vertical direction than in the lateral direction resulted in vertically aligned ZnO nanowires than planar ones.

Figure 5 illustrates the surface and vertical images of the electrodeposited ZnO nanowires with various geometries of metal film. Figure 5(a) shows electrodeposited ZnO nanowires on the Au/Ti film deposited planar Si wafer, and figures 5(b)–(d) show the electrodeposited ZnO nanowires on different geometries of Au/Ti film deposited on the nanoimprinted substrates. Nanoimprinted mother mold with a line pitch of 200 nm (figures 5(b)–(c)) and 400 nm (figure 5(d)) were utilized to fabricate nanoimprinted polymers. One metal pattern has a specific shape depending on the angle (60°) of the oblique deposition (figure 5(b)), other metal patterns were formed without oblique deposition (figures 5(a), (c), and (d)). Each diameter and density (number of ZnO nanowires per unit area) of ZnO nanowires depend on the geometry of the metal pattern, as summarized in table 1.

First, the ZnO nanowires electrodeposited on the planar metal film (figure 5(a)) were denser (density = $1.34 \times 10^6\,\mathrm{cm}^{-2}$) and thicker (average diameter = 68.97 nm (±14.41 nm)) than those synthesized on the metal patterns (average diameter = 50.69 nm (±11.63 nm), 53.27 nm (±8.63 nm), and 61.42 nm (±9.53 nm), and density = $7.6 \times 10\,\mathrm{cm}^{-2}$, $9.3 \times 10^5\,\mathrm{cm}^{-2}$, and $3.7 \times 10^5\,\mathrm{cm}^{-2}$ for ZnO nanowires deposited on each metal patterns (figures 5(b)–(d)). Second, the density and diameter of the electrodeposited ZnO nanowire could be decreased by reducing the electrochemical cathode's area. Figures 5(b) and (c) show ZnO nanowires electrodeposited on metal electrodes with different shapes. Each metal electrode has a specific shape depending on the angle of the oblique deposition. With an oblique angle of 60°, the metal electrode was only formed on the extruded polymer pattern (figure 5(b), hereafter Au60electrode), while with an oblique angle of 0°, the metal electrode was fabricated on both the extruded and recessed patterns (figure 5(c), hereafter Au0electrode). After electrodeposition of ZnO nanowires under the same conditions, the ZnO nanowires electrodeposited on the Au60electrode showed a smaller diameter and lower density than the ZnO nanowires electrodeposited on the Au0electrode. Third, the density of the ZnO nanowires decreased with an increase in the width of the recessed metal patterns. The density of the ZnO nanowires synthesized on the metal patterns with a width of 200 nm and a pitch of 400 nm (figure 5(d), hereafter Au0electrode2) was lower than that of the ZnO nanowires synthesized on the Au0electrode. The growth of the ZnO nucleus on the recessed metal patterns was considerably

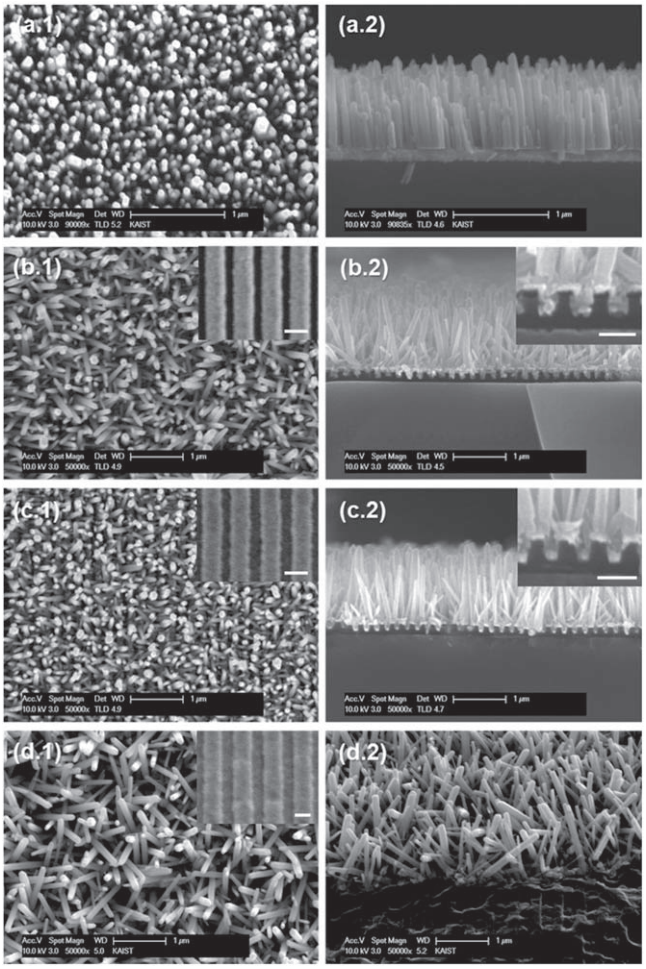

Figure 5. SEM images showing the surface and cross-section of electrodeposited ZnO nanowires on different substrates: (a.1)(a.2) Au/Ti dual-layer film deposited Si substrate, (b.1)(b.2) Au60electrode, (c.1)(c.2) Au0electrode, and (d.1)(d.2) Au0electrode2 (scale bar in the inset = 200 nm).

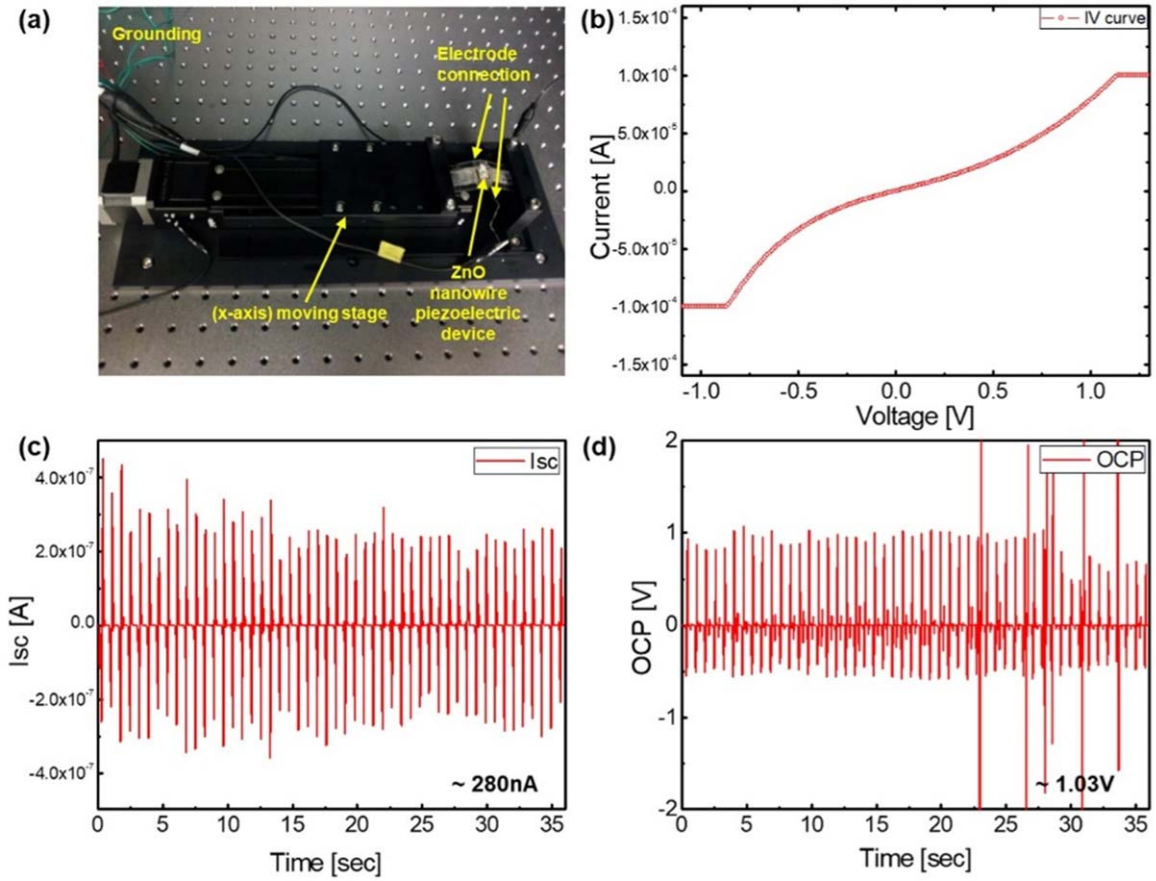

Figure 6. (a) Experimental set up for the cyclic bending test, (b) measured IV curve, (c) I_{sc}, and (d) V_{oc} of ZnO nanowires electrodeposited on Au(200 nm)/Ti(20 nm)/400 nm pitch line patterned nanoimprinted PMMA film.

Table 1. Average diameter, length, and density of ZnO nanowires electrodeposited on the (a) Au/Ti dual-layer film deposited Si substrate, (b) Au60electrode, (c) Au0electrode, and (d) Au0electrode2.

	(a) Plane Au/Ti Si-substrate	(b) Au60electrode	(c) Au0electrode	(d) Au0electrode2
Average diameter	68.97 nm (±14.41 nm)	50.69 nm (±11.63 nm)	53.27 nm (±8.63 nm)	61.42 nm (±9.53 nm)
Average length	0.77 μm (±114.97 nm)	1.07 μm (±108.81 nm)	1.17 μm (±108.48 nm)	1.06 μm (±89.78 nm)
Number of ZnO nanowires/area (Density)	1.34×10^6 cm^{-2}	7.6×10^5 cm^{-2}	9.3×10^5 cm^{-2}	3.7×10^5 cm^{-2}

limited because of the limited area of the metal pattern and disturbance by the wall of the extruded polymer patterns, resulting in a decrease in the number of ZnO nanowires.

The density and diameter of the electrochemically synthesized ZnO nanowire array structure could be controlled by changing the geometries of the metal patterns owing to the characteristics of selective ZnO nanowire deposition on the metal cathode in the electrodeposition system. Reduced density of ZnO nanowires by using this metal-nanoimprinted PMMA substrate is expected to prevent the mechanical failure of adjacent ZnO nanowires under mechanical bending. The piezoelectric and mechanical characteristics of ZnO nanowires deposited on metal-nanoimprinted PMMA films were evaluated under mechanical bending.

3.3. Piezoelectric and mechanical characteristics

The experimental setup of the vertical ZnO nanowires for the piezoelectric nanogenerators is shown in figure 6(a). The piezoelectricity of the fabricated piezoelectric nanogenerator was analyzed through a mechanical bending test ($\rho = 1$ cm, working area $= 0.75\,\text{cm}^2$). The ZnO nanowires were connected in parallel with the top (Au/Ti dual-layer thin film) and bottom electrodes (Au/Ti dual-layer thin film deposited on 400 nm pitch line patterned nanoimprinted PMMA film), resulting in Schottky contact (figure 6(b)). The open-circuit voltage (V_{oc}) and short-circuit current (I_{sc}) of the prepared piezoelectric nanogenerator were measured under a strain of 0.015 and a strain rate of $2.5\%\,\text{s}^{-1}$. The observed peak voltage and current reached 1.03 V and 280 nA (figures 6(c)

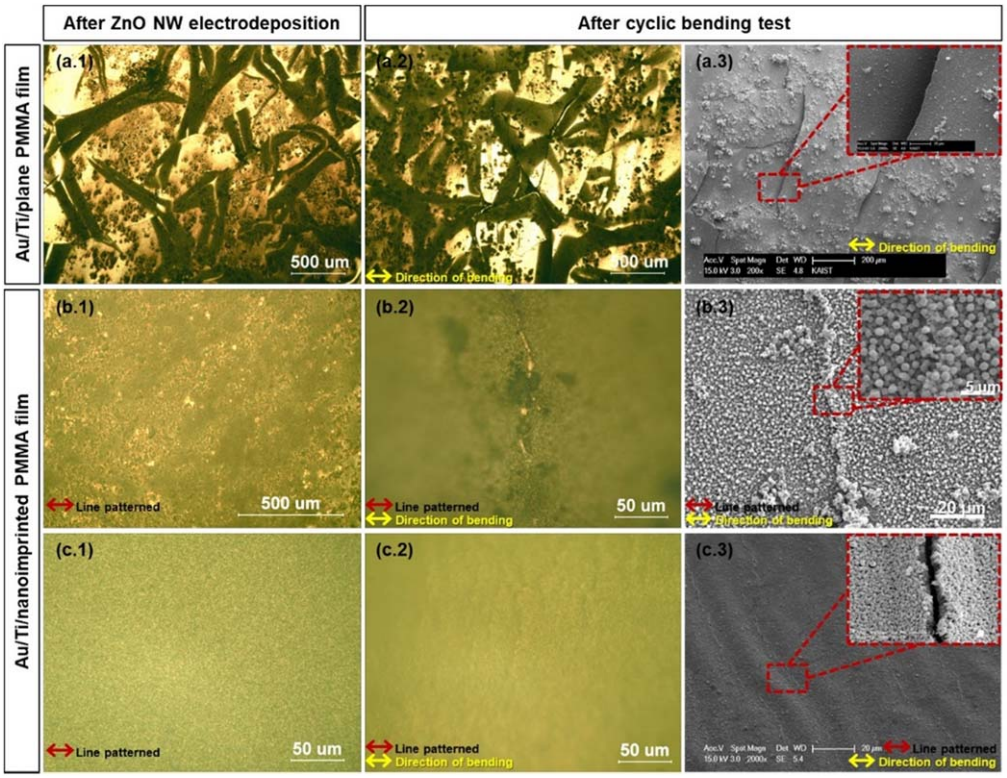

Figure 7. Optical microscope images of (a.1) as-electrodeposited ZnO nanowires on the Au/Ti/plane PMMA film, (a.2) after the bending test, and (a.3) SEM images. Optical microscope images of (b.1) as-electrodeposited ZnO nanowire on the Au/Ti/nanoimprinted PMMA film, (b.2) after the bending test, and (b.3) SEM images. Optical microscope images of (c.1) as-deposited top electrode on electrodeposited ZnO NW/Au/Ti/nanoimprinted PMMA film, (c.2) after the bending test, and (c.3) SEM images.

and (d)), respectively. These values are slightly higher than previous flexible ZnO nanowire devices fabricated by hydrothermal synthesis [18, 33], because a higher strain ($\varepsilon = 0.015$) was induced than previous study ($\varepsilon \sim 0.0019$) [33]. In addition, the ZnO nanowire device fabricated in this study exhibits superior performance compared to a previous device that incorporated a hybrid structure of ZnO nanowires and a polymer to prevent mechanical breakage [21]. Additionally, it displays comparable or even superior piezoelectric characteristics when compared to ZnO nanowire devices synthesized using a dry method [9]. Assuming that all the integrated ZnO nanowires contribute to the output, the current generated by a single ZnO nanowire is ~1.01 pA. The actual generated current from a single nanowire would be larger than that value because the strain is concentrated in the middle of the device. Wang *et al* reported that a piezoelectric field effect transistor device with a single ZnO nanowire which was fabricated by the evaporation method exhibits ~40 nA [34]. Because the high crystalline and aspect ratio of ZnO nanowire was synthesized at high temperatures by using dry-based synthesis, ZnO nanowires synthesized using dry-based methods exhibit higher piezoelectric current than those synthesized using wet-based methods. However, wet-based methods have the advantage of fabricating piezoelectric elements such as vertically integrated ZnO nanowires simply by electrodeposition on a flexible substrate at low temperatures. In the field of energy harvesting, vertically integrated nanogenerators (VING) are recognized for their efficacy in capturing compressive and bending mechanical energy [35]. The optimal transduction of mechanical deformation to piezoelectric gating on graphene (Gr) is achieved through the vertical alignment of [0001] direction-oriented ZnO nanowires, leading to remarkable sensitivity [36]. Notably, the ZnO nanowire arrays on the nanoimprinted metal substrate employed in this study exhibit a more pronounced vertical orientation compared to those on the plane metal substrate. Moreover, the controllable diameter and packing density of ZnO nanowires contribute to reducing the likelihood of mechanical breakage. In addition, ZnO nanowires can be synthesized on metal-nanoimprinted polymer in a wet chemical system and piezoelectricity can be achieved without peel-off of the bottom electrode owing to the chemical and mechanical robustness of the metal-nanoimprinted films under high moisture and mechanical bending [25].

We analyzed the adhesion characteristics of the Au/Ti/nanoimprinted PMMA film, which was the bottom electrode of the fabricated piezoelectric devices (figure 7(b.1)), and compared these characteristics with those of the piezoelectric devices formed on the Au/Ti/plane PMMA film (figure 7(a.1)). After the electrodeposition of ZnO nanowires, the Au/Ti film was delaminated from the plane PMMA substrate, while the Au/Ti film was not delaminated from the nanoimprinted PMMA film (compare figures 7(a.1) and (b.1)). The Au/Ti/nanoimprinted PMMA film has better chemical adhesion characteristics as a cathode in the electrolyte than the Au/Ti/plane PMMA film. After 1000 cycles of mechanical bending

with a radius of curvature of $\rho = 1$ cm, the Au/Ti dual-layer thin films on the plane PMMA substrate exhibited a number of cracks (length $\approx 197.09 \pm 54.18$ μm) and delaminated from the plane PMMA substrate, while the Au/Ti/nanoimprinted PMMA film had electrodeposited ZnO nanowires with smaller microcracks (length $\approx 29.74 \pm 10.67$ μm) and well attached on the nanoimprinted PMMA substrate (compare figures 7(a.2) and (b.2)). Uniform ZnO nanowire films were observed with a non-shiny color on the surface of the Au/Ti film. However, protruded shiny metal film parts were observed along with the cracks in the middle of the sample. ZnO nanowires accumulated along with these cracks (figures 7(b.2) and (b.3)). This pile-up phenomenon was observed in the middle of the flexible polymer film. This occurs as a result of stress concentrated in the middle of the flexible polymer because of the low bending rigidity of the thin PMMA substrate. After the top electrode was fabricated on ZnO nanowire film which was deposited on the Au/Ti/nanoimprinted PMMA film, similar crack propagation and pile-up phenomena were observed in the middle of the sample (compare 7b and 7c). The Au/Ti/nanoimprinted PMMA film exhibited better mechanical characteristics against bending than the Au/Ti/plane PMMA film. Therefore, vertical ZnO nanowires synthesized by using this nanoimprinted metal film without delamination under wet synthesis conditions are density-controllable and exhibit piezoelectricity during cyclic bending with a rare mechanical fracture.

4. Conclusions

In summary, we have developed a novel method for controlling the diameter and density of wet-chemically synthesized ZnO nanowire arrays using a nanoimprinted pattern metal substrate. A well-aligned vertical ZnO nanowire array structure was obtained by depositing the ZnO nanowire array structure directly on the periodic patterned metal film as the cathode in the electrochemical system. The initial growth of the ZnO nanodot-shaped nucleus played a crucial role in determining the density and diameter of the ZnO nanowire, and this process was highly dependent on the geometries of the cathode.

On the nanoimprinted metal pattern, the ZnO nucleus was generated along the surface of the extruded line pattern, while on the plane metal film, the ZnO nucleus was randomly generated. The advantage of controlling ZnO nanowire diameter and density derives from their selective growth on the extruded metal pattern and restricted growth on the recessed metal pattern. Furthermore, this controllable ZnO nanowire synthesis can be effectively carried out on the nanoimprinted metal electrode, due to its appropriate chemical adhesion characteristics in wet conditions.

In conclusion, the ZnO nanowires fabricated on the nanoimprinted metal film exhibited stable piezoelectricity with mechanical durability under cyclic bending. These results indicate the potential for manufacturing more mechanically robust flexible devices, given the use of density-controlled ZnO nanowires with high mechanical characteristics.

Acknowledgments

This work was supported by a Ministry of Culture, Sports and Tourism and Korea Creative Content Agency (ProjectNumber: R2022020033), and the Development Program of Machinery and Equipment Industrial Technology (20018235, Development of inline nano-imprinter for nano photonic device), and the Technology Innovation Program (20022462, Development of Alkaline Water Electrolysis Stack Technology) funded by the Ministry of Trade, industry and Energy(MOTIE, Republic of Korea). This work was also financially supported by the KITECH (Korea Institute of Industrial Technology) R&D Program (KITECH EO-20-0022, Development of eco-friendly production system technology for total periodic resource cycle).

Data availability statement

All data that support the findings of this study are included within the article (and any supplementary files).

Conflict of interest

The authors declare no conflicts of interest.

Ethical statement

The authors declare no ethics issue.

Authors' contributions

Hyeonjin Eom: Conceptualization, Methodology, Writing - Original Draft, Junyoung Hur: Visualization, Investigation, Sang-Keun Sung:Methodology, Investigation, Jun-Ho Jeong: Validation, Supervision, Inkyu Park: Writing—Review and Editing, Supervision, Supervision. All authors have read and approved the final manuscript.

ORCID iDs

Hyeonjin Eom https://orcid.org/0000-0003-3423-4334
Jun-Ho Jeong https://orcid.org/0000-0002-5631-3626
Inkyu Park https://orcid.org/0000-0001-5761-7739

References

[1] Xu L, Li X, Zhan Z, Wang L, Feng S, Chai X, Lu W, Shen J, Weng Z and Sun J 2015 Catalyst-free, selective growth of ZnO nanowires on SiO_2 by chemical vapor deposition for transfer-free fabrication of UV photodetectors *ACS Appl. Mater. Interfaces* **7** 20264–71
[2] Zhao Y, Li C, Chen M, Yu X, Chang Y, Chen A, Zhu H and Tang Z 2016 Growth of aligned ZnO nanowires via modified atmospheric pressure chemical vapor deposition *Phys. Lett.*A **380** 3993–7

[3] Khosravi-Nejad F, Teimouri M, Jafari Marandi S and Shariati M 2019 The highly sensitive impedimetric biosensor in label free approach for hepatitis B virus DNA detection based on tellurium doped ZnO nanowires *Appl. Phys.*A **125** 1–8

[4] Van Khai T, Van Thu L, Ha L T T, Thanh V M and Lam T D 2018 Structural, optical and gas sensing properties of vertically well-aligned ZnO nanowires grown on graphene/Si substrate by thermal evaporation method *Mater. Charact.* **141** 296–317

[5] Hosseini Z S, Zad A I and Mortezaali A 2015 Room temperature H2S gas sensor based on rather aligned ZnO nanorods with flower-like structures *Sensors Actuators*B **207** 865–71

[6] Zhang R, Pang W, Feng Z, Chen X, Chen Y, Zhang Q, Zhang H, Sun C, Yang J J and Zhang D 2017 Enabling selectivity and fast recovery of ZnO nanowire gas sensors through resistive switching *Sensors Actuators*B **238** 357–63

[7] Wang Z L and Song J 2006 Piezoelectric nanogenerators based on zinc oxide nanowire arrays *Science* **312** 242–6

[8] Lu M, Song J, Lu M, Chen M, Gao Y, Chen L and Wang Z L 2009 Piezoelectric nanogenerator using p-Type ZnO nanowire arrays *Nano Lett.* **9** 1223–7

[9] Kumar B, Lee K Y, Park H K, Chae S J, Lee Y H and Kim S W 2011 Controlled growth of semiconducting nanowire, nanowall, and hybrid nanostructures on graphene for piezoelectric nanogenerators *ACS Nano* **5** 4197–204

[10] Anthony S P, Lee J I and Kim J K 2007 Tuning optical band gap of vertically aligned ZnO nanowire arrays grown by homoepitaxial electrodeposition *Appl. Phys. Lett.* **90** 1–3

[11] Lupan O, Guérin V M, Tiginyanu I M, Ursaki V V, Chow L, Heinrich H and Pauporté T 2010 Well-aligned arrays of vertically oriented ZnO nanowires electrodeposited on ITO-coated glass and their integration in dye sensitized solar cells *J. Photochem. Photobiol.*A **211** 65–73

[12] Chevalier-César C, Capochichi-Gnambodoe M and Leprince-Wang Y 2014 Growth mechanism studies of ZnO nanowire arrays via hydrothermal method *Appl. Phys.*A **115** 953–60

[13] Pradhan D, Niroui F and Leung K T 2010 High-performance, flexible enzymatic glucose biosensor based on ZnO nanowires supported on a gold-coated polyester substrate *ACS Appl. Mater. Interfaces* **2** 2409–12

[14] Hsu C L and Chen K C 2012 Improving piezoelectric nanogenerator comprises ZnO nanowires by bending the flexible PET substrate at low vibration frequency *J. Phys. Chem.* **116** 9351–5

[15] Zi M, Zhu M, Chen L, Wei H, Yang X and Cao B 2014 ZnO photoanodes with different morphologies grown by electrochemical deposition and their dye-sensitized solar cell properties *Ceram. Int.* **40** 7965–70

[16] Xu S, Wei Y, Kirkham M, Liu J, Mai W, Davidovic D, Snyder R L and Zhong L W 2008 Patterned growth of vertically aligned ZnO nanowire arrays on inorganic substrates at low temperature without catalyst *J. Am. Chem. Soc.* **130** 14958–9

[17] Peng Y *et al* 2019 Achieving high-resolution pressure mapping via flexible GaN/ ZnO nanowire LEDs array by piezo-phototronic effect *Nano Energy* **58** 633–40

[18] Yang D, Qiu Y, Jiang Q, Guo Z, Song W, Xu J, Zong Y, Feng Q and Sun X 2017 Patterned growth of ZnO nanowires on flexible substrates for enhanced performance of flexible piezoelectric nanogenerators *Appl. Phys. Lett.* **110** 063901

[19] Wood G S, Jeronimo K, Che Mahzan M A B, Cheung R and Mastropaolo E 2021 Zinc oxide nanowires-based flexible pressure sensor *Micro Nano Lett.* **16** 432–5

[20] Rovisco A *et al* 2020 Piezoelectricity enhancement of nanogenerators based on PDMS and $ZnSnO_3$ nanowires through microstructuration *ACS Appl. Mater. Interfaces* **12** 18421–30

[21] Choi M, Murillo G, Hwang S, Kim J W, Jung J H, Chen C Y and Lee M 2017 Mechanical and electrical characterization of PVDF-ZnO hybrid structure for application to nanogenerator *Nano Energy* **33** 462–8

[22] Ong W L, Zhang C and Ho G W 2011 Ammonia plasma modification towards a rapid and low temperature approach for tuning electrical conductivity of ZnO nanowires on flexible substrates *Nanoscale* **3** 4206–14

[23] Xue F, Zhang L, Tang W, Zhang C, Du W and Wang Z L 2014 Piezotronic effect on ZnO nanowire film based temperature sensor *ACS Appl. Mater. Interfaces* **6** 5955–61

[24] Ou L X, Liu M Y, Zhu L Y, Zhang D W and Lu H L 2022 Recent progress on flexible room-temperature gas sensors based on metal oxide semiconductor *Nano-Micro Lett.* (Berlin Germany: Springer Nature) vol 14 (https://doi.org/10.1007/s40820-022-00956-9)

[25] Eom H, Kim J-H, Hur J, Kim T-S, Sung S-K, Choi J-H, Lee E, Jeong J-H and Park I 2015 Nanotextured polymer substrate for flexible and mechanically robust metal electrodes by nanoimprint lithography *ACS Appl. Mater. Interfaces* **7** 25171–9

[26] Eom H, Jung J-Y, Shin Y, Kim S, Choi J-H, Lee E, Jeong J-H and Park I 2014 Strong localized surface plasmon resonance effects of Ag/TiO core–shell nanowire arrays in UV and visible light for photocatalytic activity *Nanoscale* **6** 226–34

[27] Manzano C V, Philippe L and Serrà A 2022 Recent progress in the electrochemical deposition of ZnO nanowires: synthesis approaches and applications *Crit. Rev. Solid State Mater. Sci.* **47** 772–805

[28] Lausecker C, Salem B, Baillin X, Roussel H, Sarigiannidou E, Bassani F, Appert E, Labau S and Consonni V 2019 Formation mechanisms of ZnO nanowires on polycrystalline Au seed layers for piezoelectric applications *Nanotechnology* **30** 345601

[29] Wang Y, Rybczynski J, Wang D Z and Ren Z F 2005 Large-scale triangular lattice arrays of sub-micron islands by microsphere self-assembly *Nanotechnology* **16** 819–22

[30] Park Y C, Park B C, Romankov S, Park K J, Yoo J H, Lee Y B and Yang J M 2014 Use of permanent marker to deposit a protection layer against FIB damage in TEM specimen preparation *J. Microsc.* **255** 180–7

[31] Kim J Y, Jeong H and Jang D J 2011 Hydrothermal fabrication of well-ordered ZnO nanowire arrays on Zn foil: Room temperature ultraviolet nanolasers *J. Nanoparticle Res.* **13** 6699–706

[32] Nizar B M, Lajnef M, Chaste J, Chtourou R and Herth E 2023 Highly C-oriented (002) plane ZnO nanowires synthesis *RSC Adv.* **13** 15077–85

[33] Xu S, Qin Y, Xu C, Wei Y, Yang R and Wang Z L 2010 Self-powered nanowire devices *Nat. Nanotechnol.* **5** 366–73

[34] Wang X, Zhou J, Song J, Liu J, Xu N and Wang Z L 2006 Piezoelectric field effect transistor and nanoforce sensor based on a single ZnO nanowire *Nano Lett.* **6** 2768–72

[35] Hinchet R, Lee S, Ardila G, Montès L, Mouis M and Wang Z L 2014 Performance optimization of vertical nanowire-based piezoelectric nanogenerators *Adv. Funct. Mater.* **24** 971–7

[36] Panth M, Cook B, Zhang Y, Ewing D, Tramble A, Wilson A and Wu J 2020 High-performance strain sensors based on vertically aligned piezoelectric zinc oxide nanowire array/graphene nanohybrids *ACS Appl. Nano Mater.* **3** 6711–8